A Crosslinked Microperoxidase-11 and Nitrate Reductase Monolayer on a Gold Electrode: An Integrated Electrically Contacted Electrode for the Bioelectrocatalyzed Reduction of NO_3^-

Fernando Patolsky, Eugenii Katz, Vered Heleg-Shabtai, and Itamar Willner*

Abstract: An integrated nitrate reductase (NR) electrode is organized on a gold electrode base, to which it has electrical contact. A microperoxidase-11 (MP-11) monolayer on the electrode forms an affinity complex with NR and, upon crosslinking, generates a stable biocatalytic electrode for the electroreduction of nitrate (NO_3^-).

Keywords: biosensors · enzyme electrodes · monolayers · nitrate · redox chemistry · reductases

Introduction

The hemoprotein cytochrome *c* (cyt.*c*) acts as an electron-transfer mediator for many redox proteins. The formation of organized interprotein complexes between cyt.*c* and the protein is the key process for mediated electron transfer.[1, 2] Microperoxidase-11 (MP-11) is a heme containing 11-amino-acid oligopeptide that mimics the cyt.*c* active site microenvironment.[3] Electrochemically driven redox transformations in the presence of redox enzymes are usually prevented by the lack of electrical contact between the biocatalyst and the electrode support.[4] This results from the spatial insulation of the enzyme redox center by the surrounding protein. Hemoproteins lack direct electrical contact with the electrodes, but electron transfer may often be stimulated by appropriate modification of the electrode surface.[4, 5] Cytochrome *c* exhibits quasireversible redox features at bare glassy carbon[6] and In_2O_3 electrodes,[7] but undergoes reversible redox processes at gold, Pt, and Ag electrodes functionalized by promoter groups such as pyridine,[8] iodide,[9] thiophene,[10] or imidazole.[11] Also, negatively charged monolayers associated with electrodes have been reported to act as interfaces for appropriate alignment of cyt.*c* on electrodes; this results in electrical contact and reversible electron transfer between the hemoprotein and the electrode.[12] Electrical contact between cyt.*c* and the electrodes enables mediated biocatalyzed transformation. For example, both cytochrome *c*-mediated reduction of oxygen in the presence of cytochrome oxidase[2a,c] and the oxidation of lactate to pyruvate by lactate oxidase[2b,c] have been reported. However, these cyt.*c*-mediated transformations require the dissociation or structural reorganization of the hemoprotein from, or in respect of, the promoter sites in order to form the appropriate cyt.*c*–enzyme interprotein complexes. This intrinsic flexibility of cyt.*c*-mediated biotransformations prevents the structural rigidification of cyt.*c*–enzyme-modified electrode assemblies.

Recently, we introduced a new concept of generating integrated, bioelectrocatalytically active, enzyme electrodes through attractive interactions between electron-transfer mediators (cofactors or semisynthetic cofactors) and redox enzymes.[13] Apo-glucose oxidase was reconstituted onto a relay-FAD (flavin adenine dinucleotide) monolayer-functionalized electrode, and the resulting enzyme electrode exhibited effective direct electron transfer communication.[14] Lactate dehydrogenase and alcohol dehydrogenase both formed stable affinity complexes with a relay-NAD^+ (nicotinamide adenine dinucleotide) monolayer-functionalized electrode. The resulting cofactor–enzyme layer was crosslinked to yield a stable, integrated, electrically contacted cofactor–biocatalyst electrode.[15] A monolayer consisting of microperoxidase-11 covalently linked to a gold surface[16] was found to form affinity complexes with different hemoproteins and to mediate electron transfer.[17] For example, crosslinking of Co^{II}–protoporphyrin-reconstituted myoglobin in an affinity complex with a MP-11-functionalized electrode yields an integrated electrically contacted electrode for the bioelectrocatalyzed hydrogenation of acetylenes.[18] Here we wish to report on the organization of an integrated electrically contacted electrode for the bioelectrocatalytic reduction of nitrate. We examine the affinity complex formed between nitrate reductase (cytochrome-dependent) and a microperoxidase-11 monolayer electrode, characterize the mediated electron transfer that leads to the biocatalyzed reduction of NO_3^-, and address the chemical means to generate the

[*] Prof. I. Willner, F. Patolsky, Dr. E. Katz, V. Heleg-Shabtai
Institute of Chemistry, The Hebrew University of Jerusalem
Jerusalem 91904 (Israel)
Fax: (+972) 2-652-7715
E-mail: willnea@vms.huji.ac.il

© WILEY-VCH Verlag GmbH, D-69451 Weinheim, 1998
0947-6539/98/0406-1068 $ 17.50+.50/0 *Chem. Eur. J.* **1998**, *4*, No. 6

integrated electrode. Besides the basic interest of the characterization of interprotein electron transfer in the system, the functionalized electrode provides an active interface for the amperometric detection of nitrate (NO_3^-).

Results and Discussion

Common nitrate reductase is a NADPH-dependent enzyme that mediates the biocatalyzed reduction of nitrate (NO_3^-) to nitrite (NO_2^-). Previous reports[19] have shown that synthetic electron mediators, such as *N*,*N*′-dialkylbipyridinium radical cations, can substitute the natural cofactor and stimulate the bioelectrocatalyzed reduction of NO_3^-. Immobilization of nitrate reductase in polythiophene bipyridinium[19a] and polypyrrole bipyridinium[19b] functionalized electrodes led to the bioelectrocatalyzed reduction of NO_3^- and to the development of amperometric nitrate biosensors. A less common nitrate reductase (NR) is the cytochrome-dependent NR (E.C. 1.9.6.1) from *Escherichia coli*.[20] This enzyme utilizes cytochrome b_1 as electron-transfer mediator. The cytochrome-dependent NR is an expensive protein and its utilization in biosensor devices requires the integration of a biocatalyst in the form of effective electrically contacted layered and integrated enzyme electrodes. This was accomplished by the crosslinking of NR in an affinity complex with a MP-11-functionalized monolayer electrode.

Microperoxidase-11 was assembled on gold electrodes[16] as shown in Scheme 1. The hemooligopeptide was coupled to a base cystamine monolayer associated with the electrode. Figure 1 shows the cyclic voltammogram of the MP-11 monolayer on a roughened gold wire[21] (geometrical area

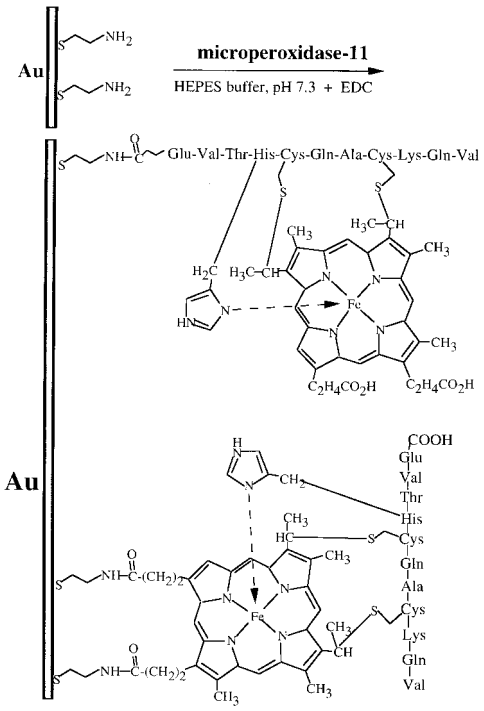

Scheme 1. Stepwise organization of the MP-11 monolayer on a gold electrode.

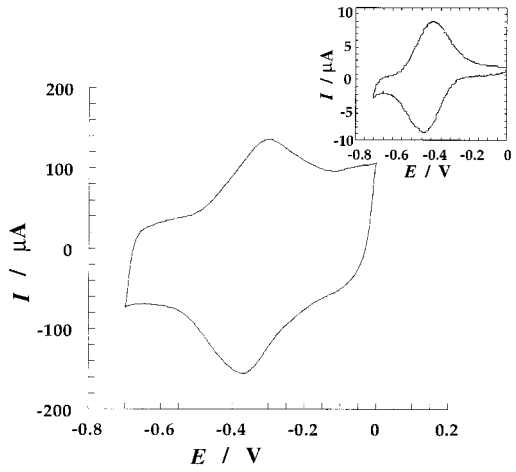

Figure 1. Cyclic voltammogram of the MP-11-monolayer-modified rough gold electrode (roughness factor ca. 15), scan rate 200 mV s^{-1}. Inset: Cyclic voltammogram of the MP-11-monolayer-modified smooth gold electrode (roughness factor ca. 1.5), scan rate 100 mV s^{-1}. Measurements were performed in 0.01 M phosphate buffer, pH = 7.0, under argon.

0.2 cm^2, roughness factor ca. 15), and (inset) on a non-roughened gold electrode (area 0.2 cm^2, roughness factor ca. 1.5). By coulometric analysis of the reduction (or oxidation) waves, we estimated the surface coverage of MP-11 on the roughened and smooth electrodes to be 1.3×10^{-10} and 2.5×10^{-10} mol cm^{-2}, respectively. In a recent study,[22] the electron transfer at the MP-11 monolayer was kinetically resolved using chronoamperometry. Two modes of covalent attachment of MP-11 in the monolayer array were revealed, including the linkage of the porphyrin carboxylic acid residues, and the oligopeptide carboxylic acid functions to the cystamine monolayer. The ratio of the MP-11 binding modes to the monolayer was estimated to be ca. 1:1.

The MP-11-functionalized electrode was used to mediate the nitrate reductase biocatalyzed reduction of nitrate (NO_3^-), Scheme 2. Figure 2 shows the cyclic voltammograms of the

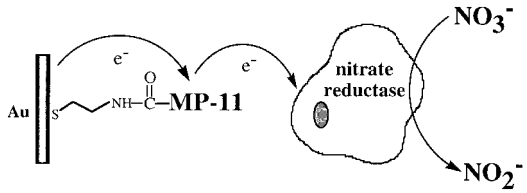

Scheme 2. Bioelectrocatalyzed reduction of NO_3^- by nitrate reductase in the presence of the MP-11-monolayer-functionalized gold electrode.

MP-11-modified electrode in the presence of NR (2.4×10^{-5} M) and nitrate (5×10^{-3} M). An electrocatalytic cathodic current is observed at the redox potential of MP-11. No electrocatalytic current is observed in the absence of NR or at a bare gold electrode in the presence of NR and NO_3^-. These results imply that MP-11 mediates the reduction of the active center of NR that stimulates the reduction of NO_3^- to nitrite (for the characterization of the NO_2^- product, vide infra). Figure 3 shows the amperometric response of the MP-11 electrode in the presence of NR (2.4×10^{-5} M) and variable concentrations of NO_3^-. The resulting current increases as

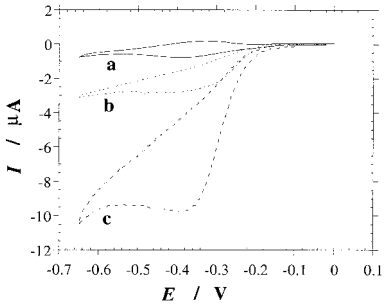

Figure 2. Cyclic voltammograms of the MP-11-modified smooth gold electrode: a) in the background electrolyte, 0.1M phosphate buffer, pH = 7.0; b) in the presence of 2.4×10^{-5}M nitrate reductase; c) in the presence of 2.4×10^{-5}M nitrate reductase and 5×10^{-3}M KNO_3. Potential scan rate 5 mV s^{-1}, under argon.

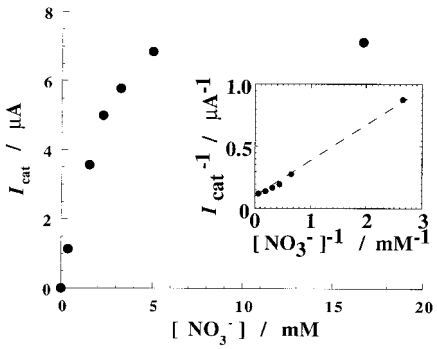

Figure 3. Electrocatalytic cathodic current developed in the presence of 2.4×10^{-5}M nitrate reductase and KNO_3 as a function of the KNO_3 concentration. Inset: Lineweaver–Burk plot for NO_3^-. Measurements were performed at MP-11-modified gold electrode in background electrolyte 0.1M phosphate buffer, pH 7.0, in chronoamperometric mode with potential steps from -0.1 to -0.5 V and current value taken 10 s after the potential step, under argon.

NO_3^- concentration is elevated and it reaches a saturation value at a NO_3^- concentration of ca. 5 mM. This is consistent with the NR active site being saturated by the substrate (NO_3^-). As the transduced current is proportional to the enzyme–substrate complex, the calibration curve shown in Figure 3 can be analyzed in terms of the Michaelis–Menten kinetic model. Figure 3 (inset) shows the Lineweaver–Burk plot of the current responses. The values $K_M = 2.4$ mM and $I_{max} = 8$ μA ($i_{max} = 30.8$ μA cm^{-2}) are derived. Thus, the MP-11 oligopeptide that represents the active site environment of cyt.*c* acts as an electron-transfer mediator for the reduction of NR and for creating the electrical contact between the biocatalyst and the electrode.

In order to understand the mechanism of MP-11-mediated reduction of NR, we examined the possible interactions between the functionalized electrode and NR by means of microgravimetric quartz-crystal microbalance (QCM) experiments. Gold electrodes associated with a quartz crystal (9 MHz, AT-cut) were functionalized by the MP-11 as outlined in Scheme 1. Figure 4 shows the frequency changes of the quartz crystal modified with MP-11 upon interaction with different concentrations of NR. The crystal frequency decreases upon addition of NR, implying a mass increase of the crystal as a result of the association of NR to the MP-11 monolayer. Furthermore, the frequency of the crystal levels

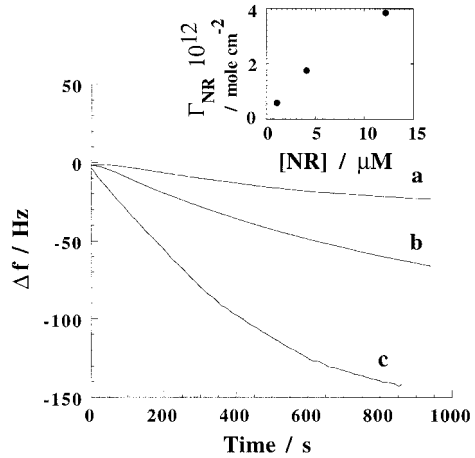

Figure 4. Time-dependent frequency changes of the MP-11-modified gold/quartz crystal in the presence of different concentrations of nitrate reductase: a) 1 μM; b) 4 μM; c) 12 μM. Inset: Steady-state, equilibrated frequency changes of the MP-11-modified gold/quartz crystal at different concentrations of nitrate reductase.

off to a constant value after ca. 900 s. The decrease in the crystal frequency is higher at elevated concentrations of NR (Figure 4, inset). These results are consistent with an equilibrium binding of NR to the MP-11 monolayer [Eq. (1)]. As

$$|-|\text{MP-11}|+\text{NR} \overset{K_a}{\rightleftharpoons} |-|\text{MP-11}|\cdots\text{NR} \quad (1)$$

the bulk concentration of NR increases, the amount of monolayer-associated NR is higher. An unmodified quartz crystal does not show significant frequency changes upon addition of NR. This indicates that the observed frequency changes for the MP-11-functionalized crystal originate from the specific associative interactions of NR with the MP-11 monolayer.

The Sauerbrey equation,[23] Equation (2), relates the crystal frequency changes Δf with the mass changes occurring on the crystal with the surface area A. Using this relation and the

$$\Delta f = -2.3 \times 10^{-6} f_o^2 \, (\Delta m/A) \quad (2)$$

molecular weight of NR ($M_r \approx 200000$), we can estimate the surface coverage of the MP-11 monolayer by NR at each bulk concentration of nitrate reductase. For example, for a bulk concentration of NR corresponding to 12 μM, the surface coverage of the MP-11 monolayer is estimated to be 3.8×10^{-12} mol cm^{-2}. As the surface coverage of MP-11 on the gold electrodes is known (1.7×10^{-10} mol cm^{-2} from QCM and 1.3×10^{-10} mol cm^{-2} from electrochemical measurements), the fraction of oligopeptide associated to the NR can be deduced and the association constant K_a can be calculated [Eq. (1)]. The value $K_a = 3.7 \times 10^3$ M^{-1} for the association of NR to the MP-11 monolayer is derived. It should be noted that addition of a different protein such as glucose oxidase to the MP-11-functionalized crystal at the concentration range used for NR did not induce any decrease in frequency. This implies that the association between MP-11 and NR originates from specific interactions.

The QCM experiments clearly reveal that interactions between NR and the MP-11 monolayer lead to their binding and to the formation of an oligopeptide–NR complex. This

© WILEY-VCH Verlag GmbH, D-69451 Weinheim, 1998
0947-6539/98/0406-1070 $ 17.50+.50/0 *Chem. Eur. J.* **1998**, *4*, No. 6

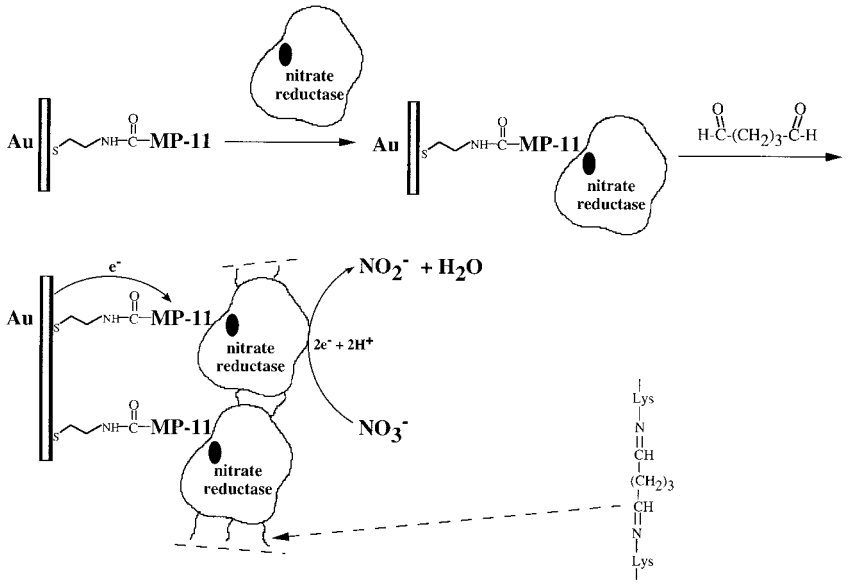

Scheme 3. Stepwise assembly of the integrated MP-11/NR-monolayer-modified gold electrode and the bioelectrocatalyzed reduction of NO_3^- at the functionalized electrode.

complex could participate in intermolecular electron transfer and thus the mediated reduction of NR. In order to characterize the kinetics of electron transfer in the complex, and because of the cost of NR, we decided to create an integrated MP-11/NR electrode (Scheme 3). Provided the affinity binding interactions between MP-11 and NR are sufficiently strong, crosslinking of the enzyme layer associated with the electrode is expected to generate a multipoint linkage between the protein and the base monolayer, and to yield a stable enzyme electrode. Accordingly, the MP-11/NR layered electrode was crosslinked with glutaric dialdehyde. Figure 5 shows the cyclic voltammogram of the resulting crosslinked assembly in the absence and in the presence of NO_3^-. An electrocatalytic cathodic current at the redox potential of MP-11 indicates the mediated bioelectrocatalyzed reduction of nitrate. The amperometric response of the electrode is stable and does not decrease over 60 minutes. This implies that the protein (NR) is not dissociated from the electrode surface and that the crosslinking yields a firm and stable electrically contacted enzyme layer. The inset in Figure 5 shows the amperometric responses of the electrode at different concentrations of nitrate. The response increases as the concentration of NO_3^- is elevated, and it levels off to a saturation current at a concentration of NO_3^- of $\approx 1.5 \times 10^{-2}$ M. The saturation current originates from the saturation of the active site of the biocatalyst with the substrate. As the transduced current is directly proportional to the rate of bioelectrocatalyzed reduction of NO_3^-, the curve shown in the inset in Figure 5 was analyzed in terms of the Michaelis–Menten model. The values $I_{max} = 47.6\ \mu A$ ($i_{max} = 15.9\ \mu A\,cm^{-2}$) and $K_M = 6.2$ mM were derived for the crosslinked NR. The higher K_M value of the crosslinked NR on the electrode support, as compared with the native, diffusing enzyme, could originate from the partial deactivation of the biocatalyst as a result of the immobilization process. It is also possible that the higher K_M value of the linked nitrate reductase originates from the crosslinking process. Transport barriers keeping the substrate from the crosslinked enzyme layer could lead to lower substrate concentrations at the enzyme interface compared with the bulk substrate concentration, thereby leading to an apparent higher K_M value.

Further mechanistic insight into the MP-11/NR-mediated reduction of nitrate was obtained by rotating disk electrode (RDE) experiments. The crosslinked MP-11/NR monolayer was assembled on a gold disk electrode, and the resulting electrocatalytic cathodic currents were determined at different concentrations of NO_3^- and variable rotation speeds, with the application of a constant potential of -0.6 V. Figure 6, curve a, shows the theoretical catalytic current at variable rotation speeds calculated by the Levich equation [Eq. (3)],[24] where n is the

$$I_{cat}(A) = 0.62\, nFAD^{2/3}\omega^{1/2}\nu^{-1/6}[NO_3^-] \quad (3)$$

number of electrons involved in the electrochemical reduction of NO_3^- (2 electrons), F

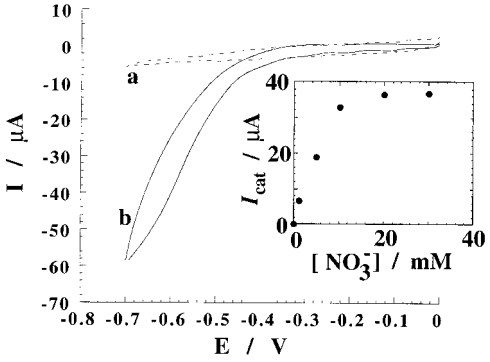

Figure 5. Cyclic voltammograms of the integrated MP-11/NR-monolayer-modified gold electrode (roughness factor ca. 15): a) vs. background solution, 0.1 M phosphate buffer, pH 7.0; b) in the presence of 20 mM KNO_3. Potential scan rate 5 mV s^{-1}. Inset: Electrocatalytic cathodic currents (measured at $E = -0.6$ V in nonstirred solution) transduced by the integrated modified gold electrode at different concentrations of KNO_3. Measurements were performed under argon.

is the Faraday constant, the real electrode area $A = 0.2$ cm^2, $D = 1.8 \times 10^5$ cm^2 s^{-1} is the diffusion coefficient[25] of NO_3^-, $\nu = 0.01$ cm^2 s^{-1} is the kinematic viscosity for water and $[NO_3^-] = 2 \times 10^{-5}$ mol cm^{-3}.

Figure 6, curve b, shows the experimental catalytic currents observed at different rotation speeds, $[NO_3^-] = 2 \times 10^{-2}$ M. The observed catalytic currents at different rotation speeds were replotted in terms of the Koutecky–Levich formulation,[24] inset in Figure 6. From the slope and intercept of the linear Koutecky–Levich plot, the interfacial electron transfer rate constant, k_{el}, was determined by means of Equation (4). For

$$k_{el} = \frac{I(\omega \to \infty)}{nFA[NO_3^-]} \quad (4)$$

example, for a concentration of $[NO_3^-] = 2 \times 10^{-2}$ M, $k_{el} = 1.05 \times 10^{-2}$ cm s^{-1} was derived. As the MP-11/NR surface

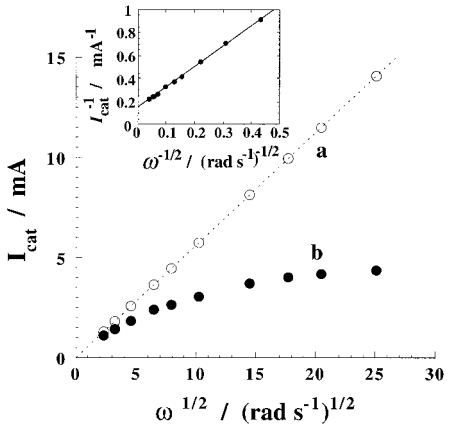

Figure 6. Electrocatalytic current corresponding to the bioelectrocatalyzed reduction of NO_3^- on the integrated MP-11/NR-monolayer-modified Au RDE vs. $\omega^{1/2}$: a) theoretical Levich plot corresponding to Eq. (3); b) experimentally measured electrocatalytic currents in the presence of 20 mM KNO_3. Background solution consists of 0.1M phosphate buffer, pH 7.0, under argon. Inset: Koutecky–Levich plot for the data shown.

density corresponds to $\Gamma = 3.8 \times 10^{-12}$ mol cm^{-2}, the overall, second-order, interfacial electron transfer, $k_{overall}$ ($k_{overall} = k_{el}/\Gamma$) corresponds to $k_{overall} = 2.8 \times 10^6$ M^{-1} s^{-1}. The $k_{overall}$ values were determined for different concentrations of NO_3^- (Figure 7). As the concentration of NO_3^- is raised, the $k_{overall}$ value

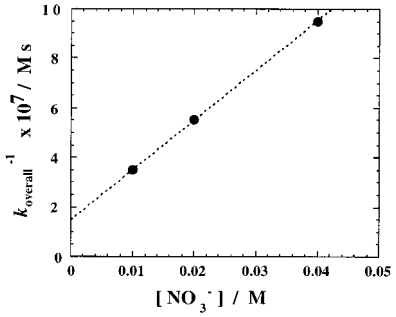

Figure 7. Second-order rate constants ($k_{overall}$) for the reduction of NO_3^- at the integrated MP-11/NR-monolayer-modified Au RDE vs. the NO_3^- concentration.

decreases, and a linear relationship between $k_{overall}^{-1}$ and $[NO_3^-]$ is observed. Note that if the electrocatalyzed reduction of NO_3^- by MP-11/NR is diffusion-controlled, then the plot $k_{overall}^{-1}$ vs. $[NO_3^-]$ should be constant (zero slope), since $k_{overall}^{-1}$ is determined at $\omega = \infty$. The nonzero slope of the $k_{overall}^{-1}$ vs. $[NO_3^-]$ plot (Figure 7) is indicative of the formation of a complex between NO_3^- and MP-11/NR, Equation (5). Ac-

$$|-\text{MP-11/NR} + NO_3^- \underset{k_{-1}}{\overset{k_1}{\rightleftharpoons}} |-\text{MP-11/NR} \cdots NO_3^- \overset{k_2}{\rightarrow} |-\text{MP-11/NR} + NO_2^- \quad (5)$$

cording to this equation, the overall electron transfer rate constant is given by Equation (6), which can be rearranged to Equation (7), where K_M is expressed by Equation (8). From

$$k_{overall} = \frac{k_2}{K_M + [NO_3^-]} \quad (6)$$

$$\frac{1}{k_{overall}} = \frac{K_M}{k_2} + \frac{1}{k_2}[NO_3^-] \quad (7)$$

$$K_M = \frac{k_2}{k_1 + k_{-1}} \quad (8)$$

the plot shown in Figure 7 we calculate $k_2 = 4.7 \times 10^4$ s^{-1} and $K_M = 6.9$ mM. This K_M value is in good agreement with the value derived from the Lineweaver–Burk plot.

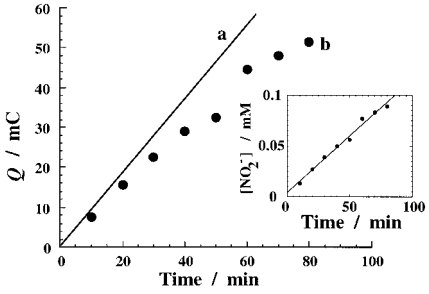

Figure 8. a) Coulometric analysis of the charge passed through the electrolytic cell during bioelectrocatalyzed reduction of NO_3^- by the integrated MP-11/NR-monolayer-modified gold electrode (roughness factor ca. 15). Electrolysis was performed in the presence of 20 mM KNO_3 in 0.1M phosphate buffer upon application of the potential -0.6 V, under argon. b) Calculated charges passed through the electrolytic cell according to analysis of the amount of the product, NO_2^-. Inset: Concentration of NO_2^- produced bioelectrochemically as a function of the electrolysis time.

A further aspect that should be addressed relates to the identification of the product (NO_2^-) formed by the bioelectrocatalyzed reduction of NO_3^-, and the application of the MP-11/NR integrated electrode for steady-state electrolysis of NO_3^-. The integrated MP-11/NR electrode was applied for the continuous electrolysis of NO_3^- by the application of a constant potential of -0.6 V to the electrode. Samples of the electrolyte were analyzed at fixed time intervals by spectroscopic determination of NO_2^-. The plot inset in Figure 8 shows the concentrations of NO_2^- produced over the period of electrolysis. Curve a in the main plot in Figure 8 shows the charge that passed through the cell during electrolysis. The amount (moles) of electrogenerated NO_2^- would require the passage of the charge shown in curve b of Figure 8. Thus the current yield for the electrocatalyzed reduction of NO_3^- to NO_2^- is ca. 85%, implying the efficient bioelectrocatalyzed reduction of nitrate by the integrated enzyme electrode.

Conclusions

We have described the construction of an integrated biocatalytic electrode for the electrocatalyzed reduction of nitrate (NO_3^-). A MP-11 monolayer assembled on a gold electrode provides an active interface to bind nitrate reductase (NR). The associative interactions are sufficiently tight to enable crosslinking of the NR layer. This process yields a stable, electrically contacted, biocatalytic electrode for the reduction of NO_3^-. The oligopeptide MP-11 mediates the reduction of NR, and the latter enzyme biocatalyzes the reduction of NO_3^- to nitrite. The current transduced by the electrode is

© WILEY-VCH Verlag GmbH, D-69451 Weinheim, 1998
0947-6539/98/0406-1072 $ 17.50+.50/0 Chem. Eur. J. 1998, 4, No. 6

controlled by the concentration of NO_3^-, and hence the integrated electrode could be applied as a nitrate biosensor.

Experimental Section

Materials: All materials, including cystamine (2,2′-diaminodiethyldisulfide) (Aldrich), 1-ethyl-3-(3-(dimethylamino)propyl)carbodiimide (EDC) (Aldrich), microperoxidase-11 (MP-11) (Sigma), and nitrate reductase (cytochrome kind, EC 1.9.6.1) from *Escherichia coli*, 5 u g^{-1} (Sigma), were used as supplied. Ultrapure water from a Nanopure (Barnstead) source was used throughout this work.

Electrode modification: Au electrodes (0.5 mm diameter Au wire, geometrical area ca. 0.2 cm^2, roughness factor ca. 1.5) were cleaned from deposited monolayers as previously described.[26] Clean Au electrodes were roughened (roughness factor ca. 15) and modified with a cystamine monolayer as reported elsewhere.[21] The freshly prepared cystamine-modified Au electrodes were used for covalent coupling with microperoxidase-11 (MP-11) in the presence of EDC.[16] Au electrodes modified with an MP-11 monolayer were incubated in nitrate reductase, 0.1 unit-mL^{-1}, in 0.1M phosphate buffer, pH = 7.0, for 15 min, rinsed briefly (2 s) with the phosphate buffer and treated with 10% (v/v) glutaric dialdehyde in water for 15 min to crosslink the adsorbed protein molecules on the electrode surface.

Measurements: Electrochemical measurements (cyclic voltammetry and amperometry under constant applied potential) used a potentiostat (EG&G VersaStat) connected to a personal computer (EG&G research electrochemistry software model 270/250). All the measurements were carried out at ambient temperature ($22 \pm 2\,^\circ$C) in a three-compartment electrochemical cell consisting of the chemically modified electrode as a working electrode, a glassy carbon auxiliary electrode isolated by a glass frit and a saturated calomel electrode (SCE) connected to the working volume with a Luggin capillary. All potentials are reported with respect to this reference electrode. Argon bubbling was used to remove oxygen from the solution in the electrochemical cell. Phosphate buffer (0.1M, pH = 7.0) was used as a background electrolyte. For all constant potential measurements (steady-state current measurements, electrolysis with spectral detection of nitrite, RDE measurements) the working electrode potential was -0.6 V.

To accumulate the reduced product (nitrite), a constant potential electrolysis was performed at an integrated MP-11/NR-monolayer electrode (a gold wire electrode with a geometrical surface area of ca. 0.2 cm^2 and a roughness factor of ca. 15). Nitrite formed upon bioelectrocatalytic reduction of nitrate was determined by a spectrometric method based on diazotization of sulfanilamide and coupling with *N*-1-naphthylethylenediamine dihydrochloride.[19a, 27] Samples (100 μL) of the cell solution were taken at intervals in a cuvette; then 1 mL of each of the reagents was added, and the absorption at $\lambda = 540$ nm was measured after 10 min.

A rotating disk electrode (RDE) (4.5 mm diameter) was polished with an alumina suspension (0.3 μm, Buehler, IL, USA), rinsed with water and then modified in the same way as the Au wire electrodes. The RDE measurements were performed with an electrode rotator (model 636, EG&G). The rate of rotation was increased stepwise and after each step the cathodic current was measured when it had stabilized (after a few seconds).

A quartz crystal microbalance analyzer (EG&G model QCA 917) linked to a personal computer was employed for the microgravimetric analysis. Quartz crystals (AT-cut, EG&G) sandwiched between two Au electrodes (area 0.196 cm^2, roughness factor ca. 3.5) were used. The fundamental frequency of the crystals was ca. 9 MHz. The crystal was mounted in a home-built flow cell ($\approx$1 mL) that included an injection septum and permitted in situ rinsing of the cell solution with an external peristaltic pump. Modification of the gold–quartz crystal with the MP-11 was done in the same way as for other gold electrodes.

Acknowledgments: This research is supported by the Israeli Ministry of Science and by the Bundesministerium für Bildung und Forschung (BMBF), Germany.

Received: October 13, 1997 [F850]

[1] M. Brunori, *Biosens. Bioelectron.* **1994**, *9*, 633–636.
[2] a) H. A. O. Hill, N. J. Walton, I. J. Wiggins, *FEBS Lett.* **1981**, *126*, 282–284; b) A. E. G. Cass, G. Davis, H. A. O. Hill, D. J. Nancarrow, *Biochim. Biophys. Acta* **1985**, *828*, 51–57; c) I. Willner, M. Lion-Dagan, S. Marx-Tibbon, E. Katz, *J. Am. Chem. Soc.* **1995**, *117*, 6581–6592.
[3] a) P. A. Adams, in *Peroxidases in Chemistry and Biology*, *Vol. 2* (Eds.: J. Everse, K. E. Everse), CRC, Boston, **1991**, ch. 7, pp. 171–200; b) G. Ranghino, G. Antonini, P. Fantucci, *Isr. J. Chem.* **1994**, *34*, 239–244.
[4] F. A. Armstrong, H. A. O. Hill, N. J. Walton, *Q. Rev. Biophys.* **1986**, *18*, 261–322.
[5] a) F. A. Armstrong, H. A. O. Hill, N. J. Walton, *Acc. Chem. Res.* **1988**, *21*, 407–413; b) J. E. Frew, H. A. O. Hill, *Eur. J. Biochem.* **1988**, *172*, 261–269.
[6] S. Dong, Q. Chi, *Bioelectrochem. Bioenerg.* **1992**, *29*, 237–245.
[7] I. Taniguchi, H. Kurihara, K. Yoshida, M. Tominaga, F. M. Hawkridge, *Denki Kagaku* **1992**, *60*, 1043–1049.
[8] a) P. M. Allen, H. A. O. Hill, N. J. Walton, *J. Electroanal. Chem.* **1984**, *178*, 69–86; b) I. Taniguchi, K. Toyosawa, H. Yamaguchi, K. Yasukouchi, *J. Chem. Soc. Chem. Commun.* **1982**, 1032–1033.
[9] T. Lu, X. Yu, S. Dong, C. Zhou, S. Ye, T. M. Cotton, *J. Electroanal. Chem.* **1994**, *369*, 79–86.
[10] X. Qu, T. Lu, S. Dong, C. Zhou, T. M. Cotton, *Bioelectrochem. Bioenerg.* **1994**, *34*, 153–156.
[11] G. Li, H. Chen, D. Zhu, *Anal. Chim. Acta* **1996**, *319*, 275–276.
[12] a) M. J. Tarlov, E. F. Bowden, *J. Am. Chem. Soc.* **1991**, *113*, 1847–1849; b) D. Hobara, K. Niki, C. Zhou, G. Chumanov, T. M. Cotton, *Colloids Surf. A: Physichochem. Engin. Aspects* **1994**, *93*, 241–250; c) T. M. Nahir, E. F. Bowden, *J. Electroanal. Chem.* **1996**, *410*, 9–13; d) S. Song, R. A. Clark, E. F. Bowden, M. J. Tarlov, *J. Phys. Chem.* **1993**, *97*, 6564–6572; e) P. N. Bartlett, D. J. Caruana, *Analyst* **1992**, *117*, 1287–1292; f) M. Collinson, E. F. Bowden, M. J. Tarlov, *Langmuir* **1992**, *8*, 1247–1250.
[13] a) I. Willner, E. Katz, B. Willner, *Electroanalysis* **1997**, *13*, 965–977; b) E. Katz, V. Heleg-Shabtai, B. Willner, I. Willner, A. F. Bückmann, *Bioelectrochem. Bioenerg.* **1997**, *42*, 95–104.
[14] I. Willner, V. Heleg-Shabtai, R. Blonder, E. Katz, G. Tao, A. F. Bückmann, A. Heller, *J. Am. Chem. Soc.* **1996**, *118*, 10321–10322.
[15] A. Bardea, E. Katz, A. F. Bückmann, I. Willner, *J. Am. Chem. Soc.* **1997**, *119*, 9114–9119.
[16] T. Lötzbeyer, W. Schuhmann, E. Katz, J. Falter, H.-L. Schmidt, *J. Electroanal. Chem.* **1994**, *377*, 291–294.
[17] A. Narvaez, E. Dominguez, I. Katakis, E. Katz, K. T. Ranjit, I. Ben-Dov, I. Willner, *J. Electroanal. Chem.* **1997**, *430*, 227–233.
[18] a) V. Heleg-Shabtai, E. Katz, I. Willner, *J. Am. Chem. Soc.* **1997**, *119*, 8121–8122; b) V. Heleg-Shabtai, E. Katz, S. Levi, I. Willner, *J. Chem. Soc. Perkin Trans. 2* **1997**, 2645–2651.
[19] a) I. Willner, E. Katz, N. Lapidot, P. Bäuerle, *Bioelectrochem. Bioenerg.* **1992**, *29*, 29–45; b) S. Cosnier, C. Innocent, Y. Jouanneau, *Anal. Chem.* **1994**, *66*, 3198–3201.
[20] a) H. Takahashi, S. Taniguchi, F. Egami, in *Comparative Biochemistry*, *Vol. 5* (Eds.: M. Florkin, H. S. Mason), Academic Press, New York, **1963**, ch. 2, pp. 91–202; b) C. H. MacGregor, in *Methods in Enzymology, Vol. 53* (Eds.: S. Fleischer, L. Packer), Academic Press, New York, **1978**, ch. 37, pp. 347–355; c) W. J. Payne, in *ibid., Vol. 53*, ch. 60, pp. 634–646.
[21] E. Katz, D. D. Schlereth, H.-L. Schmidt, *J. Electroanal. Chem.* **1994**, *367*, 59–70.
[22] E. Katz, I. Willner, *Langmuir* **1997**, *13*, 3364–3373.
[23] D. A. Buttry, in *Electroanalytical Chemistry*, *Vol. 17* (Ed.: A. J. Bard), Marcel Dekker, New York, **1991**, pp. 1–85.
[24] A. J. Bard, L. R. Faulkner, *Electrochemical Methods: Fundamentals and Applications*, Wiley, New York, **1980**.
[25] *CRC Handbook of Chemistry and Physics,* 64th ed. (Eds.: R. C. Weast, M. J. Astle, W. H. Beyer), CRC, Boca Raton, **1983**, p. F-46.
[26] E. Katz, A. A. Solov'ev, *J. Electroanal. Chem.* **1990**, *291*, 171–186.
[27] F. D. Snell, C. T. Snell, *Colorimetric Methods of Analysis,* Van Nostrand, New York, **1949**, p. 804.